

A Finite-Temperature Continuum Theory Based on Interatomic Potentials

H. Jiang

Y. Huang

Department of Mechanical and Industrial Engineering,
University of Illinois, Urbana, IL 61801

K. C. Hwang

Department of Engineering Mechanics, Tsinghua University, Beijing, China 100084

There are significant efforts to develop continuum theories based on atomistic models. These atomistic-based continuum theories are limited to zero temperature ($T=0$ K). We have developed a finite-temperature continuum theory based on interatomic potentials. The effect of finite temperature is accounted for via the local harmonic approximation, which relates the entropy to the vibration frequencies of the system, and the latter are determined from the interatomic potential. The focus of this theory is to establish the continuum constitutive model in terms of the interatomic potential and temperature. We have studied the temperature dependence of specific heat and coefficient of thermal expansion of graphene and diamond, and have found good agreements with the experimental data without any parameter fitting. We have also studied the temperature dependence of Young's modulus and bifurcation strain of single-wall carbon nanotubes. [DOI: 10.1115/1.2019865]

Keywords: Finite Temperature, Local Harmonic Approximation, Interatomic Potential, Constitutive Model

1 Introduction

There are significant efforts to develop continuum theories based on atomistic models. The quasicontinuum method [1–7] was developed to link atomistic models with the continuum finite element method in order to study the material behavior across multiple length scales. Such an approach has been used to study defects in solids [1], interfacial structure and deformation [6], and fracture and plasticity [4,5]. Shilkrot et al. [8] and Curtin and Miller [9] combined the quasicontinuum method with the discrete dislocation model to study the multiscale plastic behavior of solids. Gao and Klein [10], Klein and Gao [11,12], and Zhang et al. [13] established an approach to incorporate atomistic models into the continuum analysis, and Thiagarajan et al. [14,15] used it to study the fracture of solids. Friesecke and James [16] established a scheme for the passage from atomic to continuum theories for two-dimensional structures such as thin films, nanotubes and nanorods. Arroyo and Belytschko [17], Zhang et al. [18–21] and Jiang et al. [22] proposed nanoscale continuum theories for carbon nanotubes based on interatomic potentials for carbon. These atomistic-based continuum theories have good agreements with molecular dynamics or other atomistic simulation results. However, they are limited to zero temperature because interatomic potentials, based on how these continuum theories are established, have not accounted for the effect of finite temperature.

The temperature effect is considered in atomistic studies via several methods. One is the molecular dynamics simulation, which is a technique for computing the equilibrium and transport properties of a many-body system. Newton's equations of motion are solved for a system consisting of N particles until the properties of the system no longer change with time. The temperature is defined by using the equipartition of kinetic energy over all degrees of freedom, i.e., the instantaneous temperature is the total kinetic energy of the system divided by the number of degrees of freedom. Another method to consider the temperature effect is the Monte-Carlo simulation which computes the equilibrium properties of a system. One attempts random walking with every particle

in the system in each Monte-Carlo cycle. The energy of the system is then computed to determine whether the newly generated configuration is acceptable based on the thermodynamic principles and the sampling algorithms (accepting rate). Here the accepting rate is directly related to the probability of finding a particle point \mathbf{r} , which is proportional to the Boltzmann factor $\exp[-U(\mathbf{r})/k_B T]$, where k_B is the Boltzmann constant, T is the temperature, and U is the potential energy. The Monte Carlo cycle must be repeated a great number of times in order to sample thermodynamically relevant configurations. These atomistic methods have many advantages such as the accuracy, but they are computationally intensive and are not suitable for large scale problems.

The aforementioned atomistic-based continuum theories [17–22] do not follow every atom, and are potentially suitable for large scale problems. However, they are limited to zero temperature ($T=0$ K), and such a condition never holds for engineering problems. There exists very limited work to incorporate the temperature effect in atomistic-based continuum theories. Shenoy et al. [23] used the local harmonic approximation to calculate the Helmholtz free energy A at finite temperature. The potential energy $U(\mathbf{r})$ at zero temperature was replaced by the Helmholtz free energy $A(\mathbf{r}, T)$ in the Boltzmann factor, i.e., $\exp[-A(\mathbf{r}, T)/k_B T]$. The Monte Carlo simulation was then combined with the quasicontinuum method to determine the atom positions.

The purpose of this paper is to establish a finite-temperature continuum theory directly from the interatomic potential not involving molecular dynamics nor Monte Carlo simulation. Similar to [18–22], the interatomic potential is incorporated into the continuum analysis via the constitutive model. The effect of finite temperature is accounted for via the local harmonic approximation [24]. Such an approach has an advantage of accounting for the finite temperature effect but avoiding the use of molecular dynamics or Monte Carlo simulation.

This paper is divided into five sections. We first present the approach for an undeformed solid (i.e., vanishing strain) at finite temperature in Sec. 2. The local harmonic approximation, which is a critical step to account for the temperature effect, is also reviewed in Sec. 2. The approach for the deformed solid at finite temperature is established in Sec. 3. The continuum constitutive

Contributed by the Materials Division of ASME for publication in the JOURNAL OF ENGINEERING MATERIALS AND TECHNOLOGY. Manuscript received: January 4, 2005. Final manuscript received: March 24, 2005. Review conducted by: Min Zhou.

model is established in terms of the interatomic potential and finite temperature. We then study several temperature-dependent material properties in Sec. 4 based on Brenner's [25] interatomic potential and its second-generation potential [26] for carbon. The results are compared with the experimental data, including the coefficient of thermal expansion and specific heat of diamond and graphene, as well as the Young's modulus and bifurcation strain.

2 Finite-Temperature Analysis Based on Interatomic Potentials: Prior to Deformation

We present in this section the finite-temperature analysis for a solid prior to deformation (i.e., vanishing strain). Such an analysis paves the way for the establishment of the finite-temperature continuum theory in Sec. 3 for a deformed solid based on interatomic potentials.

2.1 Equilibrium at Zero Temperature and the Interatomic Potential. For a system of N atoms at zero temperature, the energy stored in atomic bonds is denoted by $U_{\text{tot}}(\mathbf{x}_1, \mathbf{x}_2, \dots, \mathbf{x}_N)$, where \mathbf{x}_k is the position of atom k , U_{tot} is the total potential energy of the system and is given by

$$U_{\text{tot}} = \sum_{i < j}^N V(r_{ij}; r_{ik}, k \neq i, j). \quad (1)$$

Here $V(r_{ij}; r_{ik}, k \neq i, j)$ is the multibody interatomic potential which is energy stored in the bond between atoms i and j . A multibody potential depends on not only the bond length r_{ij} , but also the lengths of other bonds $r_{ik} (k \neq i, j)$.

An example of the multibody interatomic potential is the Brenner [25] potential and the Brenner et al. [26] second-generation potential for carbon, which take the form

$$V(r_{ij}; r_{ik}, k \neq i, j) = V_R(r_{ij}) - \bar{B}_{ij} V_A(r_{ij}), \quad (2)$$

where V_R and V_A are pair terms (i.e., depending only on r_{ij}) representing the repulsive and attractive interactions between carbon atoms, respectively, \bar{B}_{ij} represents the multibody coupling which results from the interaction between atoms i, j , and their local environment. For Brenner's [25] potential,

$$V_R(r) = \frac{D^{(e)}}{S-1} e^{-\sqrt{2S}\beta[R-R^{(e)}]} f_c(r), \quad (3a)$$

$$V_A(r) = \frac{D^{(e)}S}{S-1} e^{-\sqrt{2S}\beta[R-R^{(e)}]} f_c(r), \quad (3b)$$

where $D^{(e)} = 6.000$ eV, $S = 1.22$, $\beta = 21$ nm $^{-1}$, $R^{(e)} = 0.1390$ nm, and the function f_c is merely a smooth cut-off function having the piecewise form $f_c(r) = 1, \frac{1}{2}\{1 + \cos[\pi(r - 0.17 \text{ nm})/0.03 \text{ nm}]\}$, and 0 for $r < 0.17$ nm, $0.17 \text{ nm} < r < 0.2$ nm, and $r > 0.2$ nm, respectively. The multibody coupling factor \bar{B}_{ij} in Eq. (2) is given by

$$\bar{B}_{ij} = \frac{1}{2}(B_{ij} + B_{ji}), \quad (4a)$$

$$B_{ij} = \left[1 + \sum_{k(\neq i, j)} G(\theta_{ijk}) f_c(r_{ik}) \right]^{-1/2}, \quad (4b)$$

where $\theta_{ijk} = \cos^{-1}(r_{ij}^2 + r_{ik}^2 - r_{jk}^2) / 2r_{ij}r_{ik}$ defines the angle between carbon bonds $i-j$ and $i-k$; the function G takes the form

$$G(\theta) = a_0 \left[1 + \frac{c_0^2}{d_0^2} - \frac{c_0^2}{d_0^2 + (1 + \cos \theta)^2} \right], \quad (5)$$

and $a_0 = 0.000, 208, 13$, $c_0 = 330$, $d_0 = 3.5$. The expressions of V_R , V_A , and \bar{B}_{ij} for the second-generation potential can be found in

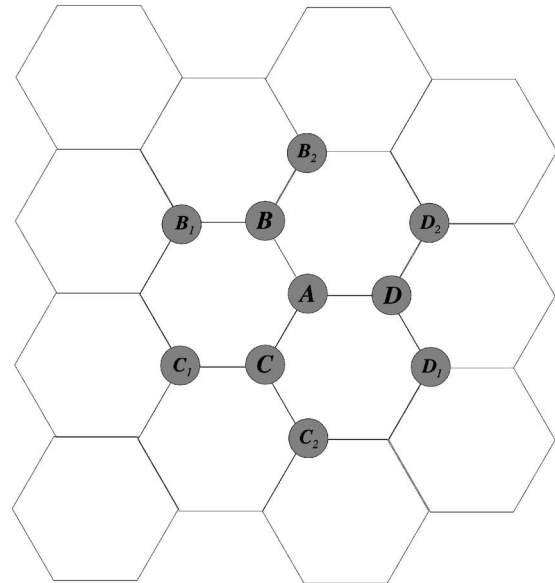


Fig. 1 A schematic diagram of the atomic structure of a graphene with a representative atom A , its three nearest-neighbor atoms B , C , and D , and six second-nearest-neighbor atoms B_1 , B_2 , C_1 , C_2 , D_1 , and D_2

[26].

The state of equilibrium at zero temperature is determined by minimizing the total potential energy in Eq. (1) with respect to atom positions, i.e.,

$$\frac{\partial U_{\text{tot}}}{\partial \mathbf{x}} = 0, \quad (6)$$

where $\mathbf{x} = (\mathbf{x}_1, \mathbf{x}_2, \dots, \mathbf{x}_N)^T$. For a periodic atomic structure that can be characterized by one (or very few) variable(s), Eq. (6) is then equivalent to the minimization of U_{tot} with respect to this (these) variable(s). For example, if all bonds have the same length r (e.g., the graphene shown in Fig. 1), the total potential energy becomes a function of r , i.e., $U_{\text{tot}} = U_{\text{tot}}(r)$. Equation (6) then becomes

$$\frac{dU_{\text{tot}}}{dr} = 0, \quad (7)$$

which determines the equilibrium bond length at zero temperature.

2.2 Equilibrium at Finite Temperature and the Local Harmonic Approximation. Atoms do not occupy stationary positions at finite (nonzero) temperature due to thermal vibrations. The center of vibration for each atom defines the "equilibrium" position at finite temperature T , i.e., the position averaged over time. The average, equilibrium bond length r at finite temperature is then the distance between the centers of vibration for nearest-neighbor atoms. It is determined by minimizing the Helmholtz free energy A , instead of the potential energy U_{tot} in Eq. (7), i.e.,

$$\frac{\partial A(r, T)}{\partial r} = 0, \quad (8)$$

where $A = U_{\text{tot}}(r) - TS$ depends on both atomic bond length r and temperature T , and S is the entropy. The equilibrium bond length is then a function of temperature T , i.e.,

$$r = r^{(0)}(T), \quad (9)$$

where the superscript 0 denotes the state prior to deformation (i.e., vanishing strain) in order to distinguish the bond length in the deformed configuration in Sec. 3.

The entropy S in the Helmholtz free energy can be calculated

from the quasiharmonic approximation, which replaces the potential energy by a harmonic expansion about equilibrium positions. Based on the quasiharmonic approximation (24), the entropy of the system of size N can be expressed as

$$S = -k_B \sum_{n=1}^{3N} \ln \left[2 \sinh \left(\frac{h\omega_n}{4\pi k_B T} \right) \right], \quad (10)$$

where k_B is the Boltzmann constant $1.38 \times 10^{-23} \text{ J K}^{-1}$, h is the Planck's constant $6.63 \times 10^{-34} \text{ J s}$, $\omega_n (n=1, 2, \dots, 3N)$ are vibration frequencies of the system and are determined from the total potential energy U_{tot} by

$$\left| \omega_n^2 \mathbf{I}_{3N \times 3N} - \frac{1}{m} \frac{\partial^2 U_{\text{tot}}}{\partial \mathbf{x} \partial \mathbf{x}} \right| = 0. \quad (11)$$

Here $\mathbf{I}_{3N \times 3N}$ is the identity matrix, m is the atomic mass, and $\mathbf{x} = (\mathbf{x}_1, \mathbf{x}_2, \dots, \mathbf{x}_N)^T$ is the position vector for all atoms.

The quasiharmonic approximation is quite accurate and gives results that are in good agreements with the Monte Carlo simulations [27]. However, the diagonalization of the $3N \times 3N$ matrix in Eq. (11) to calculate the vibration frequencies $\omega_n (n=1, 2, \dots, 3N)$ is computationally expensive. In order to avoid this difficulty, the local harmonic approximation has been introduced to neglect all terms that couple vibrations of different atoms. The effort to diagonalize the $3N \times 3N$ matrix in Eq. (11) is then reduced to the diagonalization of N 3×3 matrices, i.e.,

$$\left| \omega_{i\kappa}^2 \mathbf{I}_{3 \times 3} - \frac{1}{m} \frac{\partial^2 U_{\text{tot}}}{\partial \mathbf{x}_i \partial \mathbf{x}_i} \right| = 0, \quad i = 1, 2, \dots, N, \quad (12)$$

where $\omega_{i\kappa} (\kappa=1, 2, 3)$ are the vibration frequencies of atom i , i.e., the atom i vibrates while all other atoms are fixed at their equilibrium positions, as further illustrated in Sec. 2.3. The Helmholtz free energy is then given by [27,28]

$$A(r, T) = U_{\text{tot}}(r) + k_B T \sum_{i=1}^N \sum_{\kappa=1}^3 \ln \left[2 \sinh \left(\frac{h\omega_{i\kappa}}{4\pi k_B T} \right) \right]. \quad (13)$$

Foiles [27] evaluated the accuracy of local harmonic approximation by comparing with Monte Carlo simulation results. He concluded that, even though the local harmonic approximation somewhat underestimates the temperature dependence, it still provides a reasonable and faithful description of the trend. The results based on local harmonic approximation are acceptable at temperature below roughly one half of the melting point. Najafabadi and Srolovitz [29] investigated the influence of properties of interatomic potentials on the accuracy of local harmonic approximation. They concluded that the local harmonic approximation provides a reasonable compromise between accuracy and computational demands. However, they also pointed out that the accuracy of this approximation is sensitive to the anharmonicities in interatomic potentials.

Besides the local harmonic approximation (13), LeSar et al. [30] further introduced the high-temperature classical limit, $\sinh(h\omega_{i\kappa}/4\pi k_B T) \approx h\omega_{i\kappa}/4\pi k_B T$, such that the Helmholtz free energy in Eq. (13) becomes $A(r, T) = U_{\text{tot}} + 3k_B T \sum_{i=1}^N \ln(hD_i^{1/6}/2\pi k_B T)$, where $D_i = 1/m^3 |\partial^2 U_{\text{tot}}/\partial \mathbf{x}_i \partial \mathbf{x}_i|$ is the determinant of the local dynamic matrix. Foiles [27] conducted extensive Monte Carlo simulations and showed that this classical limit does not hold at temperature above one half of the melting temperature. This high-temperature classical limit is *not* adopted in the present study.

2.3 An Example: The Local Harmonic Approximation for Graphene. We use the graphene shown in Fig. 1 to illustrate the local harmonic approximation. The representative atom A is surrounded by three nearest-neighbor atoms $B, C,$ and D , and six second-nearest-neighbor atoms $B_1, B_2, C_1, C_2, D_1,$ and D_2 (Fig. 1). These atoms all interact with the atom A due to multibody

atomistic interactions in carbon [25,26].

2.3.1 Vibration Frequencies. We study the dependence of total potential energy on the position of the representative atom A in order to determine its vibration frequencies. The representative atom A affects not only the energy stored in three bonds $AB, AC,$ and AD at atom A , but also the energy stored in six bonds $BB_1, BB_2, CC_1, CC_2, DD_1,$ and DD_2 away from atom A [25,26]. Therefore, the total potential energy U_{tot} can be written as

$$\begin{aligned} U_{\text{tot}} = & V_{AB} + V_{AC} + V_{AD} \\ & + V_{BB_1} + V_{BB_2} + V_{CC_1} + V_{CC_2} + V_{DD_1} + V_{DD_2} \\ & + \text{bond energy independent of atom } A. \end{aligned} \quad (14)$$

Here the second line on the right-hand side is the energy which results from multibody atomistic interactions in carbon. We provide the explicit expressions for V_{AB} and V_{BB_1} in order to show their dependence on position A

$$V_{AB} = V_R(r_{AB}) - \frac{1}{2}(B_{AB} + B_{BA})V_A(r_{AB}), \quad (15)$$

$$V_{BB_1} = V_R(r_{BB_1}) - \frac{1}{2}(B_{BB_1} + B_{B_1B})V_A(r_{BB_1}), \quad (16)$$

where r_{AB} depends on position A , but r_{BB_1} does not; similarly $B_{AB}, B_{BA},$ and B_{BB_1} depend on position A via the corresponding angles involving position A , and B_{B_1B} does not.

The local dynamic matrix for graphene has only nonvanishing diagonal terms at the equilibrium position. The in-plane and out-of-plane vibration frequencies ω_1 and ω_3 can then be obtained from $\partial^2 U_{\text{tot}}/\partial x_{A_1} \partial x_{A_1}$ and $\partial^2 U_{\text{tot}}/\partial x_{A_3} \partial x_{A_3}$, respectively, and are given in the following from Brenner's [25] potential

$$\omega_1^2 = \frac{3}{2m} \left[V_R'' - B V_A'' + \frac{1}{r}(V_R' - B V_A') + \frac{\lambda_1}{r} V_A' + \frac{\lambda_2}{r^2} V_A \right], \quad (17)$$

$$\omega_3^2 = \frac{3}{m} \left[\frac{1}{r}(V_R' - B V_A') + \frac{8\lambda_1}{3r^2} V_A \right], \quad (18)$$

where $B=0.965$ is the multibody coupling factor at the equilibrium position of graphene, $\lambda_1 = B^3 3[a_0 c_0^2 / 4(d_0^2 + (1/4))^2] = 0.195$, $\lambda_2 = \lambda_1[(20/3) - B^2(3a_0 c_0^2 / 8(d_0^2 + (1/4))^2) - 5/(d_0^2 + (1/4))] = 0.607$. The vibration frequencies in Eqs. (17) and (18) are functions of the equilibrium bond length $r=r^{(0)}(T)$ at finite temperature T , and the superscript 0 denotes the state at vanishing strain.

2.3.2 Helmholtz Free Energy. The total potential energy U_{tot} can be expressed as

$$U_{\text{tot}} = N U_\varepsilon, \quad (19)$$

where N is the total number of atoms, and

$$U_\varepsilon(r) = \frac{1}{2}(V_{AB} + V_{AC} + V_{AD}) = \frac{3}{2}[V_R(r) - B V_A(r)] \quad (20)$$

is the potential energy per atom, the factor 1/2 comes from the equipartition of bond energy between two atoms in each bond, and $B=0.965$.

Based on the local harmonic approximation, the Helmholtz free energy can be written as

$$\begin{aligned} A(r, T) = & N \left\langle U_\varepsilon(r) + 2k_B T \ln \left[2 \sinh \left[\frac{h\omega_1(r)}{4\pi k_B T} \right] \right] \right. \\ & \left. + k_B T \ln \left[2 \sinh \left[\frac{h\omega_3(r)}{4\pi k_B T} \right] \right] \right\rangle. \end{aligned} \quad (21)$$

The equilibrium bond length $r=r^{(0)}(T)$ is determined by Eq. (8), i.e., minimizing the Helmholtz free energy A with respect to r .

3 Finite-Temperature Constitutive Model Based on Interatomic Potentials: Arbitrary Deformation

The finite-temperature analysis for a solid subject to arbitrary deformation is presented in this section. The analysis is also based on interatomic potentials, but it focuses on the constitutive model of the deformed solid. We first review the constitutive model based on interatomic potentials at zero temperature in Sec. 3.1, which paves the way for the constitutive model at finite temperature in Sec. 3.2.

3.1 The Constitutive Model at Zero Temperature.

3.1.1 Cauchy-Born Rule for a Centrosymmetric Atomic Structure. The continuum deformation measures can be related to the motion of many atoms via the Cauchy-Born rule [31,32], which equates the strain energy at the continuum level to the energy stored in atomic bonds. The Cauchy-Born rule also states that atoms subject to a homogeneous deformation move according to a single mapping from the undeformed to deformed configurations. Such a mapping is characterized by the continuum deformation gradient \mathbf{F} of a material point which represents the collective behavior of many atoms that undergo locally uniform deformation. For a centrosymmetric lattice structure that has a pair of bonds in opposite directions (\mathbf{r} and $-\mathbf{r}$) around each atom, the Cauchy-Born rule ensures the equilibrium of atoms because the forces in the opposite bonds are always equal and opposite.

The bond vector $\mathbf{r}_{ij}^{(0)}$ between atoms i and j prior to deformation is changed to

$$\mathbf{r}_{ij} = \mathbf{F} \cdot \mathbf{r}_{ij}^{(0)} \quad (22)$$

upon deformation, where \mathbf{F} is the continuum deformation gradient, and the superscript 0 denotes the state prior to deformation. Its length becomes

$$r_{ij}(\mathbf{E}) = \sqrt{\mathbf{r}_{ij} \cdot \mathbf{r}_{ij}} = r^{(0)} \sqrt{1 + 2\mathbf{n}_{ij}^{(0)} \cdot \mathbf{E} \cdot \mathbf{n}_{ij}^{(0)}}, \quad (23)$$

where $r^{(0)} = \sqrt{\mathbf{r}_{ij}^{(0)} \cdot \mathbf{r}_{ij}^{(0)}}$ is the bond length prior to deformation, $\mathbf{n}_{ij}^{(0)} = \mathbf{r}_{ij}^{(0)} / r^{(0)}$ is the unit vector of the bond, and $\mathbf{E} = 1/2(\mathbf{F}^T \cdot \mathbf{F} - \mathbf{I})$ is the Green strain tensor. The energy stored in bond ij is obtained from the interatomic potential in Eq. (1),

$$V(\mathbf{E}) = V[r_{ij}(\mathbf{E}); r_{ik}(\mathbf{E}), k \neq i, j], \quad (24)$$

and it depends on the Green strain \mathbf{E} .

Based on the Cauchy-Born rule, the strain energy density W on the continuum level is the energy stored in atomic bonds per unit volume of solids, and is given by

$$W(\mathbf{E}) = \frac{U_\varepsilon}{\Omega_\varepsilon} = \frac{1}{2} \frac{\sum_{1 \leq j \leq n} V[r_{ij}(\mathbf{E}); r_{ik}(\mathbf{E}), k \neq i, j]}{\Omega_\varepsilon}, \quad (25)$$

where $U_\varepsilon = (1/2) \sum_{1 \leq j \leq n} V(r_{ij}; r_{ik}, k \neq i, j)$ is the average potential energy per atom, the summation is for all (n) atoms that form bonds with the representative atom i , the factor 1/2 represents the equipartition of bond energy between two atoms in each bond; and Ω_ε is the average volume per atom.

The derivative of strain energy density W with respect to the Green strain \mathbf{E} gives the second Piola-Kirchhoff stress \mathbf{S}

$$\mathbf{S} = \frac{\partial W}{\partial \mathbf{E}}. \quad (26)$$

This gives the constitutive relation based on interatomic potentials for a centrosymmetric atomic structure at zero temperature.

3.1.2 Modified Cauchy-Born Rule for a Non-Centrosymmetric Atomic Structure. For a noncentrosymmetric atomic structure (e.g., graphene), the Cauchy-Born rule, which is based on a single mapping from the undeformed to deformed configurations, does not ensure the equilibrium of atoms anymore. For example, the graphene structure shown in Fig. 1 is not cen-

trosymmetric. The forces in bonds AB , AC , and AD do not always cancel and the net force on A may not vanish if the Cauchy-Born rule is imposed. Modifications of the Cauchy-Born rule for a non-centrosymmetric atomic structure have been proposed to ensure the equilibrium of atoms [3,17,20–22,24]. The basic idea is to decompose a noncentrosymmetric atomic structure into two (or a finite number l) sublattice structures. Each sublattice structure is centrosymmetric and follows the Cauchy-Born rule. The two (or l) sublattice structures may undergo one (or $l-1$) shift vector(s) to relax the constraint of single mapping of deformation in order to satisfy the equilibrium of atoms. In other words, the shift vector allows atoms from different sublattice structures to move differently in order to reach a minimal energy state. Accordingly, the shift vector is determined by minimizing the potential energy, which is equivalent to equilibrium.

Without losing generality, we discuss the noncentrosymmetric atomic structure that has two sublattice structures such as graphene shown in Fig. 1. The shift vector between two sublattice structures is denoted by $\boldsymbol{\zeta}$. For atoms i and j from two different sublattice structures, the bond vector \mathbf{r}_{ij} after deformation becomes

$$\mathbf{r}_{ij} = \mathbf{F} \cdot \mathbf{r}_{ij}^{(0)} + \boldsymbol{\zeta} = r^{(0)} \mathbf{F} \cdot (\mathbf{n}_{ij}^{(0)} + \boldsymbol{\xi}), \quad (27)$$

where $\boldsymbol{\xi} = (1/r^{(0)}) \mathbf{F}^{-1} \cdot \boldsymbol{\zeta}$ is an internal variable which is equivalent to the shift vector $\boldsymbol{\zeta}$. The bond length becomes

$$r_{ij}(\mathbf{E}, \boldsymbol{\xi}) = \sqrt{\mathbf{r}_{ij} \cdot \mathbf{r}_{ij}} = r^{(0)} \sqrt{(\mathbf{n}_{ij}^{(0)} + \boldsymbol{\xi}) \cdot (\mathbf{I} + 2\mathbf{E}) \cdot (\mathbf{n}_{ij}^{(0)} + \boldsymbol{\xi})}, \quad (28)$$

which depends on both the Green strain \mathbf{E} and the internal variable $\boldsymbol{\xi}$.

Similar to Eq. (19), the total potential energy is related to the potential energy U_ε per atom by $U_{\text{tot}} = NU_\varepsilon$, and U_ε is given by

$$U_\varepsilon = \frac{1}{2} \sum_{1 \leq j \leq n} V[r_{ij}(\mathbf{E}, \boldsymbol{\xi}); r_{ik}(\mathbf{E}, \boldsymbol{\xi}), k \neq i, j], \quad (29)$$

where the summation is for all (n) atoms that form bonds with the representative atom. The shift vector, or the equivalent internal variable $\boldsymbol{\xi}$, is determined by

$$\frac{\partial U_\varepsilon}{\partial \boldsymbol{\xi}} = 0. \quad (30)$$

This gives the internal variable $\boldsymbol{\xi}$ in terms of \mathbf{E} , i.e.,

$$\boldsymbol{\xi} = \boldsymbol{\xi}(\mathbf{E}). \quad (31)$$

The strain energy density in Eq. (25) now becomes

$$W(\mathbf{E}) = \frac{U_\varepsilon}{\Omega_\varepsilon} = \frac{1}{2} \frac{\sum_{1 \leq j \leq n} V[r_{ij}[\mathbf{E}, \boldsymbol{\xi}(\mathbf{E})]; r_{ik}[\mathbf{E}, \boldsymbol{\xi}(\mathbf{E})], k \neq i, j]}{\Omega_\varepsilon}, \quad (32)$$

where Ω_ε is the average volume per atom. The second Piola-Kirchhoff stress \mathbf{S} is still given by Eq. (26), $\mathbf{S} = \partial W / \partial \mathbf{E}$, but it is important to note that the internal variable $\boldsymbol{\xi} = \boldsymbol{\xi}(\mathbf{E})$ also depends on \mathbf{E} . This gives the constitutive relation based on interatomic potentials for a noncentrosymmetric atomic structure at zero temperature.

3.2 Constitutive Model at Finite Temperature.

3.2.1 Centrosymmetric Atomic Structure. The bond length at finite temperature prior to deformation is given in Eq. (9), $r = r^{(0)}(T)$. The bond vector is $\mathbf{r}_{ij}^{(0)}(T) = r^{(0)}(T) \mathbf{n}_{ij}^{(0)}$. Once the deformation is imposed, the bond vector becomes

$$\mathbf{r}_{ij} = \mathbf{F} \cdot \mathbf{r}_{ij}^{(0)}(T). \quad (33)$$

Its length is given by

$$r_{ij}(\mathbf{E}, T) = r^{(0)}(T) \sqrt{1 + 2\mathbf{n}_{ij}^{(0)} \cdot \mathbf{E} \cdot \mathbf{n}_{ij}^{(0)}}, \quad (34)$$

which depends on both Green strain \mathbf{E} and temperature T . Accordingly, the energy stored in the bond also depends on \mathbf{E} and T ,

$$V(\mathbf{E}, T) = V[r_{ij}(\mathbf{E}, T); r_{ik}(\mathbf{E}, T), k \neq i, j]. \quad (35)$$

We used the Helmholtz free energy A to replace the potential energy U_{tot} in Sec. 3.1 in order to account for the effect of finite temperature. The Helmholtz free energy in Eq. (13) can be expressed as

$$A(\mathbf{E}, T) = N \left\{ U_\varepsilon + k_B T \sum_{\kappa=1}^3 \ln \left[2 \sinh \left(\frac{h\omega_\kappa}{4\pi k_B T} \right) \right] \right\}, \quad (36)$$

where $U_\varepsilon = (1/2) \sum_{1 \leq j \leq n} V[r_{ij}(\mathbf{E}, T); r_{ik}(\mathbf{E}, T), k \neq i, j]$ is the potential energy per atom after the deformation, and it depends on the Green strain \mathbf{E} and temperature T ; ω_κ ($\kappa=1, 2, 3$) are the vibrational frequencies of the representative atom in the deformed configuration; they are still determined by Eq. (12), but they also depend on both \mathbf{E} and T .

The energy density at finite temperature is the Helmholtz free energy per unit volume [24], and is given by

$$W(\mathbf{E}, T) = \frac{A}{N\Omega_\varepsilon} = \frac{U_\varepsilon(\mathbf{E}, T) + k_B T \sum_{\kappa=1}^3 \ln \left[2 \sinh \left[\frac{h\omega_\kappa(\mathbf{E}, T)}{4\pi k_B T} \right] \right]}{\Omega_\varepsilon}. \quad (37)$$

Its derivative with respect to the Green strain \mathbf{E} gives the second Piola-Kirchhoff stress

$$\mathbf{S} = \frac{\partial W}{\partial \mathbf{E}} = \frac{1}{\Omega_\varepsilon} \frac{\partial U_\varepsilon}{\partial \mathbf{E}} + \frac{1}{\Omega_\varepsilon} \frac{h}{4\pi} \sum_{\kappa=1}^3 \coth \left[\frac{h\omega_\kappa(\mathbf{E}, T)}{4\pi k_B T} \right] \frac{\partial \omega_\kappa}{\partial \mathbf{E}}, \quad (38)$$

where the first term on the right-hand side is the same as Eq. (26) (though the bond length now depends on the temperature). The above equation gives the constitutive relation based on interatomic potentials for a centrosymmetric atomic structure at finite temperature.

3.2.2 Noncentrosymmetric Atomic Structure. Without losing generality, we discuss the noncentrosymmetric atomic structure that can be decomposed two centrosymmetric sublattice structures. The shift vector between two sublattice structures is denoted by $\boldsymbol{\zeta}$. The bond vector after deformation becomes

$$\mathbf{r}_{ij} = \mathbf{F} \cdot \mathbf{r}_{ij}^{(0)}(T) + \boldsymbol{\zeta} = r^{(0)} \mathbf{F} \cdot (\mathbf{n}_{ij}^{(0)} + \boldsymbol{\xi}), \quad (39)$$

where $\boldsymbol{\xi}$ is the equivalent internal variable. The bond length becomes

$$r_{ij}(\mathbf{E}, \boldsymbol{\xi}, T) = r^{(0)}(T) \sqrt{(\mathbf{n}_{ij}^{(0)} + \boldsymbol{\xi}) \cdot (\mathbf{I} + 2\mathbf{E}) \cdot (\mathbf{n}_{ij}^{(0)} + \boldsymbol{\xi})}. \quad (40)$$

The potential energy U_ε per atom in Eq. (29) becomes

$$U_\varepsilon = \frac{1}{2} \sum_{1 \leq j \leq n} V[r_{ij}(\mathbf{E}, \boldsymbol{\xi}, T); r_{ik}(\mathbf{E}, \boldsymbol{\xi}, T), k \neq i, j]. \quad (41)$$

The internal variable $\boldsymbol{\xi}$ is also determined by $\partial U_\varepsilon / \partial \boldsymbol{\xi} = 0$ in Eq. (30), which gives $\boldsymbol{\xi}$ in terms of the Green strain \mathbf{E} and temperature T , i.e.,

$$\boldsymbol{\xi} = \boldsymbol{\xi}(\mathbf{E}, T). \quad (42)$$

Therefore, the potential energy per atom in Eq. (41) is a function of strain \mathbf{E} and temperature T

$$U_\varepsilon = U_\varepsilon[\mathbf{E}, \boldsymbol{\xi}(\mathbf{E}, T), T]. \quad (43)$$

The Helmholtz free energy A and energy density W are still given by Eqs. (36) and (37), respectively, while Eq. (38) gives the constitutive relation based on interatomic potentials for a noncentrosymmetric atomic structure at finite temperature.

4 Applications: Temperature-Dependent Material Properties of Carbon

We use the proposed finite-temperature continuum theory based on interatomic potentials to study several temperature-dependent material properties of carbon in this section. These properties include the specific heat C_V , coefficient of thermal expansion α , Young's modulus E , and bifurcation strain.

4.1 Specific Heat. We calculate the specific heat C_V , and compare with the experimental data in order to validate the proposed finite-temperature continuum theory based on interatomic potentials. The specific heat is defined as the heat energy required per unit volume of solid per degree of temperature change. It is the sum of contributions from all vibration modes [33,34]

$$C_V = \sum_i C_{Vi}(T), \quad (44)$$

where

$$\begin{aligned} C_{Vi}(T) &= \frac{h\omega_i(T)}{2\pi V} \frac{d}{dT} \left\{ \exp \left[\frac{h\omega_i(T)}{2\pi k_B T} \right] - 1 \right\}^{-1} \\ &= \frac{h^2 \omega_i^2(T)}{16\pi^2 k_B T V} \frac{1}{\sinh^2 \left[\frac{h\omega_i(T)}{4\pi k_B T} \right]} \frac{1}{\omega_i} \frac{d\omega_i(T)}{dT}. \end{aligned} \quad (45)$$

Here the vibration frequency ω_i of the i th mode depends on temperature T via the bond length $r=r^{(0)}(T)$, h is the Planck's constant, k_B is the Boltzmann constant, and V is the total volume of the solid. Using the local harmonic approximation, we may write the specific heat in Eq. (44) as

$$C_V = \frac{h^2}{16\pi^2 k_B T \Omega_\varepsilon} \sum_{\kappa=1}^3 \left(\frac{1}{T} - \frac{1}{\omega_\kappa} \frac{d\omega_\kappa}{dT} \right) \omega_\kappa^2 \frac{1}{\sinh^2 \left(\frac{h\omega_\kappa}{4\pi k_B T} \right)} \quad (46)$$

for a solid with identical lattice structure, where Ω_ε is the volume per atom, and ω_κ ($\kappa=1,2,3$) are three vibration frequencies of the representative atom.

The specific heat is usually presented in the literature by the heat energy required per mole of atoms per degree of temperature change [35,36]. Therefore, Eq. (46) becomes

$$C_V = \frac{6.022 \times 10^{23} h^2}{16\pi^2 k_B T} \sum_{\kappa=1}^3 \left(\frac{1}{T} - \frac{1}{\omega_\kappa} \frac{d\omega_\kappa}{dT} \right) \omega_\kappa^2 \frac{1}{\sinh^2 \left(\frac{h\omega_\kappa}{4\pi k_B T} \right)}, \quad (47)$$

where 6.022×10^{23} is the number of atoms per mole.

For the graphene shown in Fig. 1, two in-plane vibration frequencies $\omega_1 = \omega_2$ are given in Eq. (17), and the out-of-plane frequency ω_3 is given in Eq. (18). Figure 2 shows the specific heat (per mole of atoms) versus temperature for graphene predicted by the present theory based on Brenner's [25] interatomic potential for carbon. The results based on the Brenner et al. [26] second-generation potential are also shown, together with the experimental data of graphite [36]. It is observed that, without any parameter fitting, the specific heat predicted by the present analysis for graphene agrees very well with the experimental data for graphite over the entire range of temperature.

Figure 3 shows the specific heat (per mole of atoms) versus temperature for diamond based on Brenner's [25] potential and the Brenner et al. [26] second-generation potential. The experimental data [35] are also shown for comparison. Once again the present analysis based on Brenner's [25] potential agrees very well with the experimental data, while the results based on the Brenner et al. [26] second-generation potential are lower than the

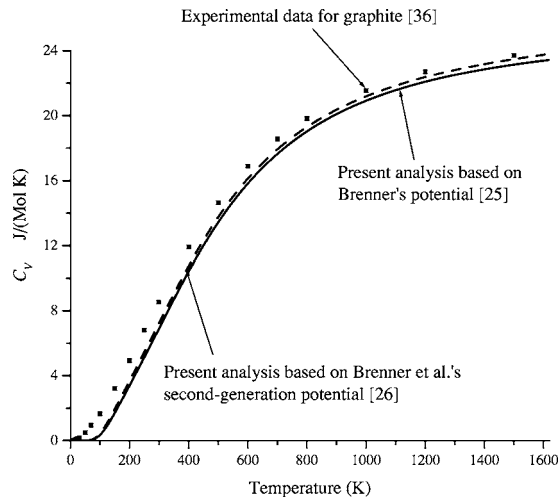


Fig. 2 Temperature dependence of specific heat C_v for graphene predicted by the present continuum theory based on interatomic potentials. The experimental data of graphite [36] are also shown.

experimental data.

The numerical results show that, for both graphene and diamond, the $1/T$ term dominates the numerator in Eqs. (46) and (47), i.e., $1/T \gg 1/\omega_\kappa (d\omega_\kappa/dT)$, such that the contribution from the derivative of frequencies $d\omega_\kappa/dT$ is negligible. This observation is important for excellent agreement between the present analysis and experimental data, and will be further explained in the next section.

4.2 Coefficient of Thermal Expansion. We study the coefficient of thermal expansion (CTE) α via the finite-temperature continuum theory based on interatomic potentials. The CTE is the fractional change in the linear dimension of solid per degree of temperature change, and is related to the bond length $r=r^{(0)}(T)$ in Eq. (9) by

$$\alpha = \frac{1}{r^{(0)}(293 \text{ K})} \frac{dr^{(0)}(T)}{dT}, \quad (48)$$

where $dr^{(0)}(T)/dT$ can be obtained from $\partial A/\partial r=0$ in Eq. (8) as

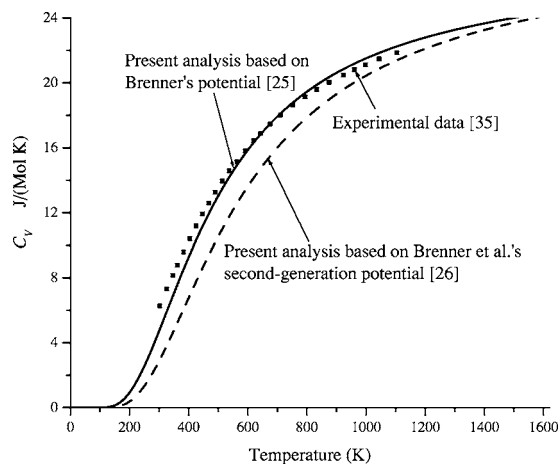


Fig. 3 Temperature dependence of specific heat C_v for diamond predicted by the present continuum theory based on interatomic potentials. The experimental data [35] are also shown.

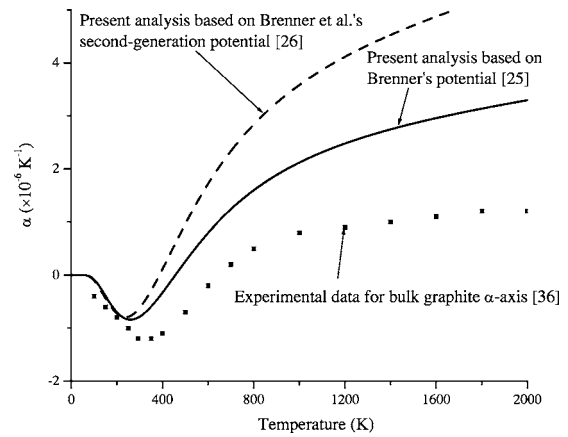


Fig. 4 Temperature dependence of the coefficient of thermal expansion α for graphene predicted by the present continuum theory based on interatomic potentials. The experimental data of graphite [36] are also shown.

$$\frac{dr^{(0)}(T)}{dT} = - \left. \frac{\frac{\partial^2 A}{\partial r \partial T}}{\frac{\partial^2 A}{\partial r^2}} \right|_{r=r^{(0)}(T)}. \quad (49)$$

Here

$$A = N \left\langle U_\varepsilon(r) + k_B T \sum_{\kappa=1}^3 \ln \left[2 \sinh \left[\frac{h\omega_\kappa(r)}{4\pi k_B T} \right] \right] \right\rangle \quad (50)$$

is the Helmholtz free energy based on the local harmonic approximation, and U_ε is the potential energy per atom. The derivative $\partial^2 A/\partial r \partial T$ in Eq. (49) is then obtained as

$$\frac{\partial^2 A}{\partial r \partial T} = N \frac{h^2}{16\pi^2 k_B T^2} \sum_{\kappa=1}^3 \left. \frac{\omega_\kappa \frac{d\omega_\kappa}{dr}}{\sinh^2 \left[\frac{h\omega_\kappa(r)}{4\pi k_B T} \right]} \right|_{r=r^{(0)}(T)}. \quad (51)$$

For a harmonic potential, $\omega_\kappa = \text{constant}$, the above equation gives vanishing $\partial^2 A/\partial r \partial T$ and therefore vanishing CTE in Eq. (48). This means that the thermal expansion results from the anharmonicity of the interatomic potential.

Figure 4 shows the predicted CTE of graphene versus temperature based on Brenner's [25] potential and the Brenner et al. [26] second-generation potential. The in-plane and out-of-plane vibration frequencies of graphene are given in Eqs. (17) and (18), respectively. The experimental data for α -axis CTE of graphite [36] are also shown in Fig. 4 for comparison. It is observed that, without any parameter fitting, the CTE predicted by the present analysis for graphene agrees reasonably well with the experimental data for graphite. However, the difference between the predicted and experimental data for CTE in Fig. 4 is larger than that for specific heat shown in Fig. 2. This discrepancy is mainly because the CTE is directly proportional to the derivative of vibration frequencies $d\omega_\kappa/dr$ as observed from Eqs. (48), (49), and (51). It is recalled from Eq. (12) that ω_κ is obtained from the second-order derivative of the interatomic potential. Therefore, $d\omega_\kappa/dr$ involves the third-order derivatives of the potential energy, which may not be accurate since the parameters in interatomic potentials are usually determined from the energy at the ground state, its first-order derivative (lattice constant) and second-order derivative (elastic moduli), but not third-order derivative [25,26].

It is interesting to note that the specific heat given in Eqs. (46) and (47) also involves the third-order derivative of the potential energy via $d\omega_\kappa/dT$, but the agreement between the specific heat predicted by the present analysis and experimental data (Fig. 2) is much better than that for the CTE (Fig. 4). This is because, as

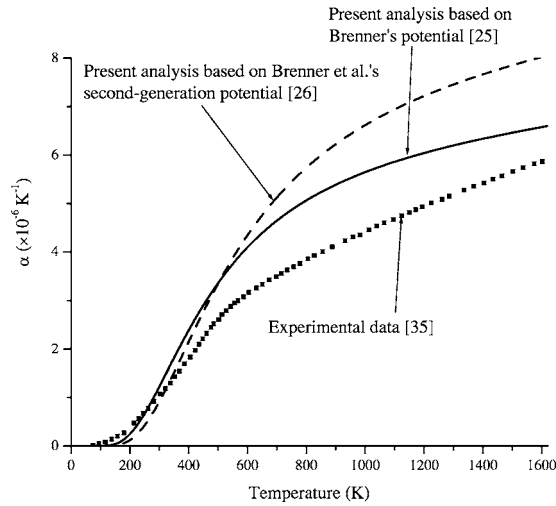


Fig. 5 Temperature dependence of the coefficient of thermal expansion α for diamond predicted by the present continuum theory based on interatomic potentials. The experimental data [35] are also shown.

discussed at the end of Sec. 4, the contribution from $d\omega_\kappa/dT$ to the specific heat C_V is negligible as compared to $1/T$ in Eqs. (46) and (47) such that C_V is essentially independent of $d\omega_\kappa/dT$.

It is observed that the predicted CTE of graphene is negative for temperature $T < 456$ K for Brenner's [25] potential (and $T < 386$ K for the Brenner et al. [26] second-generation potential). Jiang et al. [37] have shown that single wall carbon nanotubes also have negative CTE at low and room temperature. This negative CTE is due to the negative contribution from the out-of-plane vibration frequency. Our numerical results have shown that $d\omega_1/dr < 0$, $d\omega_3/dr > 0$, and $\omega_1 = \omega_2$ are at least an order of magnitude larger than ω_3 , i.e., $\omega_1 \gg \omega_3$. As the temperature approaches zero $T \rightarrow 0$, Eq. (51) is dominated by the contribution from ω_3 and is given by $\frac{\partial^2 A}{\partial r \partial T} \approx N(h^2/4\pi^2 k_B T^2) \omega_3(d\omega_3/dr) / \exp[h\omega_3(r)/2\pi k_B T] > 0$ such that $\alpha < 0$, as seen from Eqs. (48) and (49). The experimental data for graphite also show negative α -axis CTE for a large range of temperature.

Figure 5 shows that CTE versus temperature for diamond based on Brenner's [25] potential and the Brenner et al. [26] second-generation potential. The experimental data [35] are also shown for comparison. Without any parameter fitting, the present analysis based on Brenner's [25] potential captures the temperature dependence of the CTE, though the agreement with the experimental data is not as good as that for the specific heat (see Figs. 3 and 5). This is once again because the CTE is proportional to the third-order derivative of the potential energy.

The results in Figs. 2 and 3 for specific heat suggest that the local harmonic approximation captures the finite temperature effect very well. However, the use of the third-order derivative of the interatomic potential may lead to inaccuracies, as evidenced by the discrepancies in CTE between the theory and experimental data in Figs. 4 and 5.

4.3 Young's Modulus. We study the temperature dependence of Young's modulus and Poisson's ratio of graphene via the present finite-temperature continuum theory based on interatomic potentials. The incremental modulus tensor \mathbf{C} , which relates the stress rate and strain rate by $\dot{\mathbf{S}} = \mathbf{C} : \dot{\mathbf{E}}$, is given by

$$\mathbf{C} = \frac{\partial^2 W[\mathbf{E}, \xi(\mathbf{E}, T), T]}{\partial \mathbf{E} \partial \mathbf{E}}. \quad (52)$$

For the limit of vanishing strain $\mathbf{E} = 0$, the above equation gives

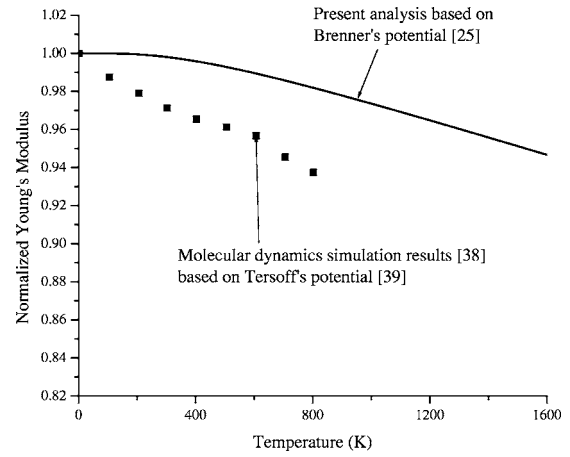


Fig. 6 Temperature dependence of Young's modulus for graphene predicted by the present continuum theory based on interatomic potentials. Here the Young's modulus is normalized by its counterpart at zero temperature. The molecular dynamics simulation results for a (10,10) carbon nanotube [38] based on a different interatomic potential [39] are also shown.

the linear elastic modulus tensor.

Let x_1 and x_2 denote the Cartesian coordinates in the plane of graphene, and x_3 the out-of-plane direction. It can be verified that the nonvanishing components of \mathbf{C} are $C_{1111} = C_{2222}$, $C_{1122} = C_{2211}$, $C_{1212} = C_{1221} = C_{2112} = C_{2121}$ at vanishing strain $\mathbf{E} = 0$. The Young's modulus and in-plane Poisson's ratio are given by

$$E = C_{1111} - \frac{C_{1122}^2}{C_{1111}}, \quad \nu = \frac{C_{1122}}{C_{1111}}. \quad (53)$$

Here the Young's modulus E is actually the linear elastic stiffness with the dimension of Newton/meter. This is because the graphene thickness is not well defined such that the volume Ω_ε per atom in Eqs. (37) and (38) is replaced by the area per atom.

Figure 6 shows the Young's modulus of graphene versus the temperature. The Young's modulus has been normalized by its counterpart at zero temperature in order to avoid the ambiguity in thickness. The Young's modulus decreases with the increasing temperature, though the amount of decrease is relatively small. Therefore, the Young's modulus is insensitive to temperature, which is not unexpected for linear elastic properties. The variation of Poisson's ratio is relatively small, from $\nu = 0.41$ for $T = 0$ to $\nu = 0.40$ for $T = 1600$ K. This once again confirms that the linear elastic properties are insensitive to temperature.

Figure 6 also shows the temperature dependence of Young's modulus for a (10,10) carbon nanotube obtained by molecular dynamics simulations [38] based on a different interatomic potential for carbon [39]. It is observed that the Young's modulus given by molecular dynamics decreases faster with the increasing temperature than that given by the present continuum theory. There can be several factors that are responsible for this difference. First, different interatomic potentials are used, namely the Tersoff potential [39] in molecular dynamics and Brenner potential [25,26] in the continuum theory. Second, the molecular dynamics simulations are for a (10,10) carbon nanotube, while the present continuum theory is for a graphene. Third, the local harmonic approximation may underestimate the temperature effect.

4.4 Bifurcation Strain of Single-Wall Carbon Nanotubes. Zhang et al. [21] investigated the bifurcation of a single-wall carbon nanotube (CNT) under tension at zero temperature, and found that the bifurcation strain predicted by the continuum theory based on interatomic potentials agrees well with the breaking strain of CNT obtained from atomistic simulations [40–42]. We extend the

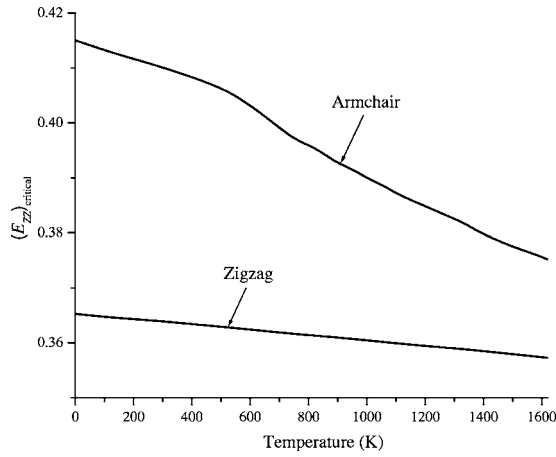


Fig. 7 Temperature dependence of bifurcation strain $(E_{ZZ})_{\text{critical}}$ predicted by the present continuum theory based on interatomic potentials for armchair and zigzag carbon nanotubes under tension

Zhang et al. [21] analysis to finite temperature in this section.

For a single-wall CNT subject to uniaxial tension along the tube axis, the deformation in the CNT is uniform until the axial strain reaches a critical value to trigger bifurcation. This represents the onset of nonuniform deformation in the CNT. Let (R, θ, Z) be the cylindrical coordinates for the CNT. Zhang et al. [21] established the critical condition for bifurcation in armchair and zigzag CNTs [43] as

$$C_{\theta\theta\theta\theta} \left(C_{ZZZZ} + \frac{S_{ZZ}}{1 + 2E_{ZZ}} \right) - C_{\theta\theta ZZ}^2 + \frac{S_{ZZ}}{1 + 2E_{\theta\theta}} \left(C_{ZZZZ} + \frac{S_{ZZ}}{1 + 2E_{ZZ}} \right) \times \left(\frac{m\pi R}{L} \right)^2 = 0, \quad (54)$$

where R and L are the radius and length of CNT, respectively; $m=1, 2, 3, \dots$, is the eigen mode number; S_{ZZ} is the only nonvanishing component of the second Piola-Kirchhoff stress; the nonvanishing components of the Green strains E_{ZZ} and $E_{\theta\theta}$ are related by the uniaxial tension condition $S_{\theta\theta}=0$, and C is the incremental modulus tensor in Eq. (52). The above bifurcation condition also holds at finite temperature, though the stress S_{ZZ} , strain $E_{\theta\theta}$, and moduli C depend on both the axial strain E_{ZZ} and temperature T .

For infinitesimal strain $E_{ZZ} \rightarrow 0$, the left-hand side of Eq. (54) becomes $(C_{\theta\theta\theta\theta} C_{ZZZZ} - C_{\theta\theta ZZ}^2)|_{E=0}$, which is always positive. As the strain increases, the left-hand side decreases and eventually reaches zero, which corresponds to the onset of bifurcation and the corresponding strain is denoted by $(E_{ZZ})_{\text{critical}}$. The above procedure is repeated for all possible eigen mode $m=1, 2, 3, \dots$, though our results show that the lowest mode ($m=1$) always gives the smallest bifurcation strain.

Figure 7 shows the bifurcation strain $(E_{ZZ})_{\text{critical}}$ for armchair and zigzag CNTs under tension. The CNT radius is $R=0.5$ nm, and length $L=5$ nm. The bifurcation strain at zero temperature $T=0$ agrees well with the breaking strain of CNT (see Zhang et al. [21]). As temperature increases, the bifurcation strain decreases, and it decreases faster for the armchair CNTs than zigzag CNTs. Even though this decrease of bifurcation strain with increasing temperature is reasonable, the magnitude of decrease in Fig. 7 is small. This is mainly because the present analysis based on interatomic potentials is static, and has not accounted for the kinetic energy associated with the atom vibration at finite temperature.

5 Concluding Remarks and Discussion

We have developed a finite-temperature continuum theory based on interatomic potentials. The effect of finite temperature is

accounted for via the local harmonic approximation, which relates the entropy to the vibration frequencies of the system, and the latter are determined from the interatomic potential. The focus of this theory is to establish the continuum constitutive model in terms of the interatomic potential and temperature. We have studied the temperature dependence of specific heat and coefficient of thermal expansion of graphene and diamond, and have found good agreements with the experimental data without any parameter fitting. We have also studied the temperature dependence of Young's modulus and bifurcation strain of single-wall carbon nanotubes.

The finite-temperature continuum theory based on interatomic potentials can also be combined with the atomistic methods such as the quasicontinuum method [1–7] or atomic-scale finite element method (AFEM) [44,45] to study the temperature-dependent behavior of materials. For example, the combination of AFEM and present continuum theory provides a means to study materials behavior across multiple length scales. AFEM can be applied to domains where the behavior of discrete atoms is important (e.g., around a crack tip), while the atomistic-based continuum theory can be applied to domains where materials can be modeled as continuum (e.g., far away from the crack tip). Such a combination is unique in that both AFEM and present continuum theory are consistently based on the same interatomic potential.

Acknowledgments

Y.H. acknowledges insightful discussions with W. A. Curtin of Brown University, and the support from NSF (Grant Nos. 00-99909, 01-03257, and the Nano CEMMS Center at UIUC), Office of Naval Research (Grant No. N00014-01-1-0205, Program Manager Dr. Y. D. S. Rajapakse), Alexander von Humboldt Foundation, and NSFC. K.C.H. acknowledges support from NSFC and the Ministry of Education, China.

References

- [1] Tadmor, E. B., Ortiz, M., and Phillips, R., 1996, "Quasicontinuum Analysis of Defects in Solids," *Philos. Mag. A* **73**, pp. 1529–1563.
- [2] Tadmor, E. B., Phillips, R., and Ortiz, M., 1996, "Mixed Atomistic and Continuum Models of Deformation in Solids," *Langmuir* **12**, pp. 4529–4534.
- [3] Tadmor, E. B., Smith, G. S., Bernstein, N., and Kaxiras, E., 1999, "Mixed Finite Element and Atomistic Formulation for Complex Crystals," *Phys. Rev. B* **59**, pp. 235–245.
- [4] Miller, R., Ortiz, M., Phillips, R., Shenoy, V., and Tadmor, E. B., 1998, "Quasicontinuum Models of Fracture and Plasticity," *Eng. Fract. Mech.*, **61**, pp. 427–444.
- [5] Miller, R., Tadmor, E. B., Phillips, R., and Ortiz, M., 1998, "Quasicontinuum Simulation of Fracture at the Atomic Scale," *Modell. Simul. Mater. Sci. Eng.*, **6**, pp. 607–638.
- [6] Shenoy, V. B., Miller, R., Tadmor, E. B., Phillips, R., and Ortiz, M., 1998, "Quasicontinuum Models of Interfacial Structure and Deformation," *Phys. Rev. Lett.* **80**, pp. 742–745.
- [7] Shenoy, V. B., Miller, R., Tadmor, E. B., Rodney, D., Phillips, R., and Ortiz, M., 1999, "An Adaptive Finite Element Approach to Atomic-Scale Mechanics—The Quasicontinuum Method," *J. Mech. Phys. Solids* **47**, pp. 611–642.
- [8] Shilkrot, L. E., Curtin, W. A., and Miller, R. E., 2002, "A Coupled Atomistic/Continuum Model of Defects in Solids," *J. Mech. Phys. Solids* **50**, pp. 2085–2106.
- [9] Curtin, W. A., and Miller, R. E., 2003, "Atomistic/Continuum Coupling in Computational Materials Science," *Modell. Simul. Mater. Sci. Eng.*, **11**, pp. R33–R68.
- [10] Gao, H., and Klein, P. A., 1998, "Numerical Simulation of Crack Growth in an Isotropic Solid with Randomized Internal Cohesive Bonds," *J. Mech. Phys. Solids* **46**, pp. 187–218.
- [11] Klein, P. A., and Gao, H., 1998, "Crack Nucleation and Growth as Strain Localization in a Virtual-Bond Continuum," *Eng. Fract. Mech.*, **61**, pp. 21–48.
- [12] Klein, P. A., and Gao, H., 2000, "Study of Crack Dynamics Using the Virtual Internal Bond Method," *Multiscale Deformation and Fracture in Materials and Structures, James R. Rice's 60th Anniversary Volume*, Kluwer Academic Publishers, Dordrecht, The Netherlands, pp. 275–309.
- [13] Zhang, P., Klein, P., Huang, Y., Gao, H., and Wu, P. D., 2002, "Numerical Simulation of Cohesive Fracture by the Virtual-Internal-Bond Model," *Comput. Model. Eng. Sci.*, **3** pp. 263–277.
- [14] Thiagarajan, G., Hsia, K. J., and Huang, Y., 2004, "Finite Element Implementation of Virtual Internal Bond Model for Crack Behavior Simulation," *Eng. Fract. Mech.*, **71**, pp. 401–423.
- [15] Thiagarajan, G., Huang, Y., and Hsia, K. J., 2004, "Fracture Simulation Using

- an Elasto-Viscoplastic Virtual Internal Bond Model with Finite Elements,” *J. Appl. Phys.* **71**, pp. 796–804.
- [16] Friesecke, G., and James, R. D., 2000, “A Scheme for the Passage from Atomic to Continuum Theory for Thin Films, Nanotubes and Nanorods,” *J. Mech. Phys. Solids* **48**, pp. 1519–1540.
- [17] Arroyo, M., and Belytschko, T., 2002, “An Atomistic-Based Finite Deformation Membrane for Single Layer Crystalline Films,” *J. Mech. Phys. Solids* **50**, pp. 1941–1977.
- [18] Zhang, P., Huang, Y., Gao, H., and Hwang, K. C., 2002, “Fracture Nucleation in Single-Wall Carbon Nanotubes Under Tension: A Continuum Analysis Incorporating Interatomic Potentials,” *ASME J. Appl. Mech.* **69**, pp. 454–458.
- [19] Zhang, P., Huang, Y., Geubelle, P. H., and Hwang, K. C., 2002, “On the Continuum Modeling of Carbon Nanotubes,” *Acta Mech. Sin.* **18**, pp. 528–536.
- [20] Zhang, P., Huang, Y., Geubelle, P. H., Klein, P. A., and Hwang, K. C., 2002, “The Elastic Modulus of Single-Wall Carbon Nanotubes: A Continuum Analysis Incorporating Interatomic Potentials,” *Int. J. Solids Struct.*, **39**, pp. 3893–3906.
- [21] Zhang, P., Jiang, H., Huang, Y., Geubelle, P., and Hwang, K., 2004, “An Atomistic-Based Continuum Theory for Carbon Nanotubes: Analysis of Fracture Nucleation,” *J. Mech. Phys. Solids* **52**, pp. 977–998.
- [22] Jiang, H., Zhang, P., Liu, B., Huang, Y., Geubelle, P. H., Gao, H., and Hwang, K. C., 2003, “The Effect of Nanotube Radius on the Constitutive Model for Carbon Nanotubes,” *Comput. Mater. Sci.*, **28**, pp. 429–442.
- [23] Shenoy, V., Shenoy, V., and Phillips, R., 1999, “Finite Temperature Quasicontinuum Methods,” *Mater. Res. Soc. Symp. Proc.* **538**, pp. 465–471.
- [24] Weiner, J. H., *Statistical Mechanics of Elasticity* (Wiley, New York, 1983).
- [25] Brenner, D. W., 1990, “Empirical Potential for Hydrocarbons for Use in Simulating the Chemical Vapor Deposition of Diamond Films,” *Phys. Rev. B* **42**, pp. 9458–9471.
- [26] Brenner, D. W., Shenderova, O. A., Harrison, J. A., Stuart, S. J., Ni, B., and Sinnott, S. B., 2002, “A Second-Generation Reactive Empirical Bond Order (Rebo) Potential Energy Expression for Hydrocarbons,” *J. Phys.: Condens. Matter* **14**, pp. 783–802.
- [27] Foiles, S. M., 1994, “Evaluation of Harmonic Methods for Calculating the Free Energy of Defects in Solids,” *Phys. Rev. B* **49**, pp. 14930–14938.
- [28] Chandler, D., *Introduction to Modern Statistical Mechanics* (Oxford University Press, Oxford, 1987).
- [29] Najafabadi, R., and Srolovitz, D. J., 1995, “Evaluation of the Accuracy of the Free-Energy-Minimization Method,” *Phys. Rev. B* **52**, pp. 9229–9241.
- [30] LeSar, R., Najafabadi, R., and Srolovitz, D. J., 1989, “Finite-Temperature Defect Properties from Free-Energy Minimization,” *Phys. Rev. Lett.* **63**, pp. 624–627.
- [31] Born, M., and Huang, K., 1954, “*Dynamical Theory of the Crystal Lattices*,” Oxford University Press, Oxford.
- [32] Milstein, F., 1980, “Review: Theoretical Elastic Behaviour at Large Strains,” *J. Mater. Sci.*, **15**, pp. 1071–1084.
- [33] Ashcroft, N. W., and Mermin, N., 1976, *Solid State Physics*, Saunders College, Philadelphia.
- [34] Ashcroft, N. W., and Mermin, N., 1981, *Solid State Physics*, Holt-Saunders, Japan, Tokyo.
- [35] *Physics of Group IV Elements and III-V Compounds*, 1982, edited by Madelung Landolt-Börnstein, New Series, Group III, Vol. 17, Springer-Verlag, Berlin.
- [36] Billings, B. H., and Gray, D. E., 1972, *American Institute of Physics Handbook*, McGraw-Hill, New York.
- [37] Jiang, H., Liu, B., Huang, Y., and Hwang, K. C., 2004, “Thermal Expansion of Single Wall Carbon Nanotubes,” *ASME J. Eng. Mater. Technol.*, **126**, pp. 265–270.
- [38] Raravikar, N. R., Keblinski, P., Rao, A. M., Dresselhaus, M. S., Schadler, L. S., and Ajayan, P. M., 2002, “Temperature Dependence of Radial Breathing Mode Raman Frequency of Single-Walled Carbon Nanotubes,” *Phys. Rev. B* **66**, p. 235424.
- [39] Tersoff, J., 1988, “Empirical Interatomic Potential for Carbon, with Applications to Amorphous Carbon,” *Phys. Rev. Lett.* **61**, pp. 2879–2882.
- [40] Yakobson, B. I., Campbell, M. P., Brabec, C. J., and Bernholc, J., 1997, “High Strain Rate Fracture and C-chain Unraveling in Carbon Nanotubes,” *Comput. Mater. Sci.* **8**, pp. 341–348.
- [41] Ogata, S., and Shibutani, Y., 2003, “Ideal Tensile Strength and Band Gap of Single-Walled Carbon Nanotubes,” *Phys. Rev. B* **68**, p. 165409.
- [42] Mielke, S., Troya, D., Zhang, S., Li, J. L., Xiao, S., Car, R., Ruoff, R. S., Schatz, G. C., and Belytschko, T., 2004, “The Role of Vacancy Defects and Holes in the Fracture of Carbon Nanotubes,” *Chem. Phys. Lett.* **390**, pp. 413–420.
- [43] Saito, R., Dresselhaus, G., and Dresselhaus, M. S., 1998, *Physical Properties of Carbon Nanotubes*, Imperial College Press, London.
- [44] Liu, B., Huang, Y., Jiang, H., Qu, S., and Hwang, K. C., 2004, “The Atomic-Scale Finite Element Method,” *Comput. Methods Appl. Mech. Eng.* **193**, pp. 1849–1864.
- [45] Liu, B., Jiang, H., Huang, Y., Qu, S., Yu, M. F., and Hwang, K. C., “Atomic-Scale Finite Element Method in Multiscale Computation with Applications to Carbon Nanotubes,” *Phys. Rev. B* (to be published).